Substantial meltwater contribution to the Brahmaputra revealed by satellite gravimetry

Shuang Yi[1,2,*], Chunqiao Song[3], Kosuke Heki[2], Shichang Kang[4], Qiuyu Wang[5], Le Chang[5]

[1]Institute of Geodesy, University of Stuttgart, 70174 Stuttgart, Germany
5 [2]Department of Earth and Planetary Sciences, Hokkaido University, Sapporo, Japan
[3]Key Laboratory of Watershed Geographic Sciences, Nanjing Institute of Geography and Limnology, Chinese Academy of Sciences, Nanjing, 210008, China.
[4]State Key Laboratory of Cryospheric Sciences, Cold and Arid Regions Environmental and Engineering Research Institute, Chinese Academy of Sciences, Lanzhou 730000, China
10 [5]Key Laboratory of Computational Geodynamics, University of Chinese Academy of Sciences, Beijing 100049, China;

Correspondence to: Shuang Yi (shuangyi.geo@gmail.com)

Abstract. High Asia glaciers were observed to be reducing the fastest in the southeastern Tibet Plateau (SETP), where vast amounts of glacier and snow (GS) feed the streamflow of the Brahmaputra, a transboundary river linking the world's two most
15 populous countries China and India. However, the low temporal resolutions in previous studies obscured the seasonal accumulation/ablation variations, and their modelling estimates were divergent. Here we use monthly satellite gravimetry observations from August 2002 to June 2017 to estimate GS mass variation in the SETP. We find that the "spring-accumulation type" glaciers and winter snow in the SETP are the most abundant in May. This is in stark contrast to seasonal variations in terrestrial water storage, which reaches its maximum in August and is controlled by summer precipitation. These two seasonal
20 variations are mutually orthogonal and can be easily separated in time-variable gravity observations. Our results show a summer meltwater contribution of 43±8 Gt to the Brahmaputra. This value could help to resolve previous divergent modelling estimates and underlines the importance of meltwater to the Brahmaputra streamflow. The high sensitivity between GS melting and temperature on both annual and monthly scales suggests that the Brahmaputra will suffer from not only changes in total annual discharge, but also an earlier runoff peak due to the ongoing global warming.

25 # 1 Introduction

The Tibetan Plateau, regarded as the Asian water tower, is the source of several major river systems. Their upper streams are fed by rainfall, base flow and widespread glaciers and snow (GS) melt (Barnett et al., 2005; Immerzeel et al., 2010; Jansson et al., 2003). The sustainable supply of GS melt, which is susceptible to climate change, is the key to the local freshwater security, flood prevention and control, and hydroelectric development (Bolch et al., 2012; Kaser et al., 2010; Yao et al., 2012).
30 The southeastern Tibet Plateau (SETP), including the Nyenchen Tonglha Mountains (NTM) and eastern Himalayas, holds 10,439 glaciers with a total area of 9,679 km² (RGI Consortium, 2017) and widespread snow coverage. These maritime glaciers are characterized by low equilibrium-line altitudes with large topographic gradients (Yao et al., 2012) and the most severe mass loss in High Mountain Asia (HMA) (Brun et al., 2017; Kääb et al., 2015). The GS melt serves as an essential water

supplier for the Brahmaputra river system (e.g., Immerzeel et al., 2010; Lutz et al., 2014), which runs through three densely
35 populated countries, China, India and Bangladesh (Figure 1). The manifesting vulnerability of glaciers in the Brahmaputra
Basin to global warming and emerging controversies over water allocation (e.g., dam building (Tanck and Fazani, 2010)) are
increasingly attracting scientific and public concern.

Due to the lack of observational data, most of the previous estimates on the contribution of seasonal meltwater to the
upstream flow of the Brahmaputra River were based on modelling approaches that were only calibrated by the streamflow,
40 and the absence of direct constraints on GS mass balance leads to a wide range from 19% to 35% in their estimates (Table 1)
due to different forcing data and approaches (Bookhagen and Burbank, 2010; Chen et al., 2017; Huss et al., 2017; Immerzeel
et al., 2010; Lutz et al., 2014; Zhang et al., 2013). The amount of meltwater could be even more divergent. For example, Huss
et al. (2017) estimated that the amount of annual GS melt to the Brahmaputra River was 138 w.e. (water equivalent) km^3 yr^{-1},
which is however triple the estimate of 43 w.e. km^3 yr^{-1} by Lutz et al. (2014). Such huge discrepancies in previous estimates
45 make the inclusion of calibration from GS mass balance observations an urgent task.

Spaceborne sensors can be helpful in this desolate mountain region. Remote sensing techniques for region-wide GS mass
balance measurements can be divided into three categories: laser altimetry (e.g., Ice, Cloud and land Elevation Satellite
(ICESat) (Kääb et al., 2012)), multi-temporal digital elevation models (e.g., SPOT (Gardelle et al., 2013), ASTER (Brun et al.,
2017)), and space gravimetry (Gravity Recovery and Climate Experiment (GRACE) (Matsuo and Heki, 2010; Yi and Sun,
50 2014)). The first two employ geodetic approach (glacier surface height variation), and we need to determine the average ice
density to convert volume changes into mass changes. The ICESat observation suffers from short operation period (2003–
2009) and sparse spatial sampling, both of which can be overcome by the stereo-imagery approach. However, the stereo-
imagery strategy has only recently been applied to the entire HMA region. Brun et al. (2017) provided an estimate of the
detailed glacier mass balance trends over HMA between 2000 and 2016 and highlighted the regional dissimilarity. Despite
55 recent improvements in spatial resolution in HMA glacier mass change studies, there has been little advance in their temporal
resolution. This is even more crucial for calibration and validation of glaciological models.

Observations of monthly time resolution are necessary to separately quantify summer and winter mass balances, two
processes dominating the annual glacier mass balance (Cogley et al., 2011). The amplitude of seasonal variation of the glaciers
in the SETP is up to ~3 m w.e. (Wang et al., 2017), far exceeding their net annual change of ~ 0.6 m w.e. (Brun et al., 2017).
60 Hence, the long-term trend of GS mass changes only reflects a small net imbalance of their ablation and accumulation. High
time-resolution monthly observations by GRACE since its launch in 2002 (Tapley et al., 2004) are promising in identifying
these two processes. Up to now, the application of GRACE in HMA glaciers has been focusing on their secular changes with
little attention to the seasonal variations (Gardner et al., 2013; Matsuo and Heki, 2010; Yi and Sun, 2014). This is partly due
to the poor spatial resolution of GRACE (> 300 km) and to the dominance of terrestrial hydrological signals in the seasonal
65 gravity signals, which is difficult to separate from glacial signals. The latter is particularly severe in regions with intense
monsoon precipitation such as the SETP. The seasonal GS and hydrological mass changes (mainly including mass changes in
rivers, soil moisture and groundwater) dominate the regional gravity signals observed by GRACE. Despite the general

difficulty in separating them in the spatial domain, we find it possible to separate the two signals in the time domain in the SETP, owing to their contrasting seasonal behaviours.

Precipitation in the SETP is controlled by various atmospheric circulation systems in different seasons, with westerly winds and Bay of Bengal vortex in winter/spring and Indian monsoon in summer (Wu et al., 2011; Yang et al., 2013; Yao et al., 2012). The former two systems were found to drive the spring precipitation in the SETP along the Brahmaputra River, thus forming a 'spring-accumulation' type of glaciers (Yang et al., 2013). The Indian monsoon prevails from June to September and brings intense precipitation on the southern side of the Himalayas, where terrestrial water storage shows tremendous seasonal changes and peaks in late summer. Therefore, we can observe two peaks in the precipitation seasonality based on the climatological stations near the NTM (Yang et al., 2013).

In this work, we will first introduce the precipitation characteristics of this region by both meteorological stations and global precipitation products. We will then use the empirical orthogonal function (EOF) analysis to decompose hydrological and GS signals. After obtaining the GS signal, the monthly GS mass balance will be compared to the glacier mass balance measured from ICESat. Such high time-resolution observations also allow us to compare GS mass variations with temperature records during the ablation season, and to study the sensitivity of GS in response to the temperature. Finally, we will compare our results to previous estimates on a monthly, annual, and interannual scales.

2 Data

2.1 GRACE data and preprocessing

We adopt the monthly GRACE spherical harmonics Release 06 products from August 2002 to June 2017. The three datasets are solved respectively by three organizations: Center for Space Research (CSR) at the University of Texas, GeoForschungsZentrum (GFZ) in Potsdam, and the Jet Propulsion Laboratory (JPL). These datasets are available at ftp://podaac.jpl.nasa.gov/allData/grace/L2/. The degree 1 terms, which are absent in original GRACE releases, have been added based on the technique proposed by Swenson et al. (2008). The C_{20} terms have been replaced by those from satellite laser ranging (Cheng et al., 2011), which are considered to be more reliable. A widely used Glacial Isostatic Adjustment (GIA) model by A et al. (2013) is adopted to correct the GIA effect caused by historical polar ice sheet changes.

Two different filtering strategies, a combination of P4M6 decorrelation (Swenson and Wahr, 2006) and 300km Gaussian filter (hereafter short for G300+P4M6) and a DDK4 filter (Kusche et al., 2009), are applied separately. Therefore, there are six combinations and their average values (with uniform weights) are given. The standard deviations among these six datasets are taken as the uncertainties of the mass estimate, assuming that other sources of uncertainty are negligible.

2.2 ICESat altimetry

Version 34 of the ICESat Global Land Surface Altimetry Data is used to derive glacier height changes. The data span is from 2003 to 2009, with two or three observation campaigns per year (Figure S1). The processing of ICESat data includes the

following steps. (1) Orthometric heights are obtained from original elevation data based on the Earth's gravity model 2008.
100 (2) Footprints on glaciers are identified based on RGI 6.0 glacier outlines. (3) For each ICESat footprint, SRTM (Farr et al., 2007) elevations and slopes are extracted by bilinear interpolation of the DEM grid cells. Glacier height variation is defined as the elevation differences between the footprints and the SRTM data. (4) We exclude footprints over SRTM voids, footprints with slopes higher than 30°, and footprints with height change larger than 100 m (which are attributed to biases caused by cloud cover during the ICESat acquisition). (5) We also discard the calibration campaign L1AB (March 2003) and the
105 incomplete campaign L2F (October 2009). (6) Glacier height variations are averaged and interpolated along the altitude to alleviate the uneven sampling problem in space, and an uncertainty of 0.06 m/yr (Kääb et al., 2012) is chosen to account for the uneven sampling bias in time. The steps have been used in previous work (Wang et al., 2017) and have also been described in earlier studies (Gardner et al., 2013; Kääb et al., 2012). The footprint information is given in Fig. S2.

ICESat has shown good ability to solve snow variation in flat regions (Treichler and Kääb, 2017), but applying the same
110 technique in mountainous areas with high terrain heterogeneity is cumbersome. Therefore, here ICESat is only used to estimate changes in glacier mass. Although our GRACE estimate includes both glaciers and snow, the estimates by GRACE and ICESat are comparable in the late ablation season (i.e., the October/November campaign of ICESat), when the contribution of seasonal snow meltwater is negligible. To convert the glacier thickness changes into mass changes, two parameters are required, i.e., glacier density and total glacier areas. We assume an average glacier density of 850 ± 60 kg m^{-3} (Huss, 2013). According to
115 the glacier inventory RGI 6.0 (RGI Consortium, 2017), the area has a glacierized area of 9,679 km^2.

2.3 Other auxiliary data

There are four meteorological stations in this mountainous area. Their locations are labelled in Figure S3 and their spatial information is listed in Table S1. Precipitation and temperature records for each site from 2003 to 2016 (Figure S4) are available from the China Meteorological Data Service Center (http://data.cma.cn/data/weatherBk.html). To maintain
120 consistency, the site temperature is converted to an elevation of 5500 m (averaged equilibrium line altitude) by a lapse rate of -0.006 ℃/m (Li et al., 2013). This conversion has little effect on the results of this study as only temperature anomalies are used.

Moderate-resolution imaging spectroradiometer (MODIS) data MOD10 (Hall et al., 2006) is used to investigate snow coverage here. The MOD10CM product has a temporal resolution of 1 month and spatial resolution of 0.05-degree.
125 The land surface model Global Land Data Assimilation System (GLDAS)-NOAH (Rodell et al., 2004) is adopted to inspect soil moisture changes, which can be compared to changes in total terrestrial water storage estimated by GRACE. Here, the version 2.1 monthly product with 1.0-degree spatial resolution is used (available at https://hydro1.gesdisc.eosdis.nasa.gov/data/GLDAS/GLDAS_NOAH10_M.2.1/).

Global gridded precipitation data Tropical Rainfall Measuring Mission (TRMM) (Huffman et al., 2014) is used to
130 examine the influence of precipitation on water storage. The data is available at https://pmm.nasa.gov/data-access/downloads/trmm. Although such a global product is unable to capture the localized spring precipitation in our study

area (shown later), it can be used for the investigation of large-scale monsoon precipitation. We also use High Asia Refined analysis (HAR) precipitation product generated using the atmospheric model WRF (Maussion et al., 2014). In this product, long-term precipitation trends are not recommended, but its 10 km spatial resolved seasonal variation is informative to
135   investigate the spatial extent of spring precipitation. The HAR data is available at http://www.klima-ds.tu-berlin.de/har/.

3 Spring precipitation and mass increase

The method of this study is based on the fact that spring precipitation driven glacial/snow mass changes earlier than hydrological signals. Therefore, before introducing the method, we want to demonstrate that spring precipitation and its associated mass changes are detectable by GRACE. At two of four stations (Bomi and Chayu), spring precipitation is
140   noticeable, even surpassing the summer/autumn precipitation brought by the Indian monsoon (Figure S4). Yang et al. (2013) provided precipitation records for 22 sites in a broader area. Based on these data, they outlined the boundary of the impact zone of the spring precipitation, which roughly covers the glacierized area studied here. Summer precipitation and its associated hydrological mass change are enormous and well recognized, so here we only show the spring precipitation evolving from January to March by TRMM and HAR in Figure 2. The precipitation begins to spread south and westward since April, when
145   the monsoons gradually increase (not shown here). The TRMM results show a boundary along the latitude 29° N, and the precipitation in the north suddenly decreases. This reduced boundary is irrelevant to terrain and seems to be artificial. This phenomenon cannot be found in the HAR result, which clearly shows abundant precipitation in the glacierized zone in these months. The bottom gives the GRACE monthly mass anomalies from March to May (two months later than the precipitation), because we found such a time lag in the response of mass change to precipitation. An earlier mass increase from April can be
150   identified in the southeastern part of the Tibetan Plateau.

Our station measurements evaluate the performance of TRMM and HAR in Figure S5. According to the measurements of our observatory, the spring precipitation of the Bomi and Chayu stations is obvious, and bimodal changes can be identified. TRMM is capable of revealing the condition of Chaya at 28.65° N, but it does not perform well in regions north of 29° N. The HAR data do not represent a good bimodal change, which seems to slightly underestimate the precipitation in April and
155   overestimate in Autumn and Winter.

These results show that spring precipitation can be captured more or less by various measurements/products and the 'spring-accumulation' pattern of SETP glaciers can be recognized in GRACE observations. The amplitude and phase of the seasonal mass variation from the equivalent water height (EWH) of GRACE are compared in the background of Figure 1. The spatial distribution of the seasonal amplitude is similar to the influence zone of the Indian monsoon. This pattern reflects the
160   predominance of the monsoon-controlled hydrological process and the weaker glacial signals in this region. However, the peak month of seasonal changes (the contours in Figure 1) shows a distinct pattern, with peaks in June in the NTM and appearing later as we go south. The peak comes in August in the southern Himalayas, where the annual amplitude reaches its maximum. The shift in peak months reflects the increasing/decreasing contribution from the sinusoid of the hydrological/GS seasonal

variation. A key point should be pointed out is that their peaks have a three-month time window shift (we will demonstrate it
165 later), that is one-fourth of the annual oscillation period and means that the two signals are mathematically orthogonal.

4 Decomposition of GRACE signals

4.1 EOF analysis of GRACE

GS and hydrological mass changes dominate the seasonal gravity signals observed by GRACE in this region and they
are mathematically orthogonal by different phases. Therefore, we employ the EOF technique (see the supporting material for
170 mathematic expressions) (Björnsson and Venegas, 1997) to decompose hydrological and glacial signals in the six combinations
of three GRACE datasets by two filters, and the average result is illustrated in Figure 3. We thus extract two modes which
have an explained variance higher than the other modes (i.e., two significant modes are obtained). Comparing the results of
different datasets and filters, they show good consistency, indicating that the first two modes are robust.

Each mode consists of one EOF (the spatial pattern) and one PC (the temporal evolution). Only the first two modes are
175 presented, and they explain $79 \pm 5\%$ and $12 \pm 4\%$ of the total variance, respectively. Although overall, the first mode is much
stronger than the second mode (because the second mode is more localized), their signal strength in the glacierized region is
comparable on both seasonal and secular temporal scales. Modes above 2 are weak and irregular and show a lot of noise, so
they are discarded here.

The trends of the GRACE observation and its decomposed modes are shown in Figure 4. GRACE observations show
180 significant mass loss, which is split into the first two modes. In the glacierized zone, $\sim 2/3$ of the negative trend comes from
the 2nd mode and $\sim 1/3$ comes from the 1st mode. The trend of higher modes (> 2) is quite weak (Figure 4d).

According to the spatial coverage (EOF_1 and EOF_2) and their temporal variation (PC_1 and PC_2), the first mode covering
the low altitude areas on the south of the plateau with a peak month in August/September seemingly represents hydrologic
signals and the second mode concentrating in the glacierized region with a peak month in May seemingly represents glaciers.

4.2 GS mass estimation from mode 2

We choose the second mode to estimate GS mass change. The EOF_2 only shows a smooth mass pattern and we need
some strategy to recover its original mass. To this end, a forward modelling method (Yi et al., 2016) is chosen to iteratively
recover the mass in an pre-defined region. This method has been widely used (Chen et al., 2015; Wouters et al., 2008),
especially in the study of polar ice sheets. In the first step, we divide the glacier mask based on the glacier distribution recorded
190 in RGI 6.0 (RGI Consortium, 2017) (Figure 4e). The lattices have a resolution of $0.5°$ by $0.5°$ and are located in glacierized
area. In the second step, the mass in each lattice is iteratively adjusted until its smoothing signal (Figure 4f) well matches the
GRACE observation (Figure 4c). The details of each combination of datasets and filters are presented in Figure S6 and S7.
Therefore, we solve the mass in each combination (Figure S7). The mass is multiplied by the PC_2 series to derive the glacier
mass series, and their average is taken as the mass estimate.

4.3 Validation of mode 1 by soil moisture and precipitation datasets

To validate the hypothesis that the first mode represents hydrological signals, we apply EOF analysis to two other datasets, soil moisture from GLDAS/NOAH and precipitation data from TRMM (Figure 5). To make them comparable to GRACE in terms of spatial resolution, they are expanded into spherical harmonics, truncated at degree 60, and smoothed by the same filter. Their results are shown in Figure 5. Different from GRACE that has two significant modes, they only have one, due to the lack of a glacial signal. The EOF_1 of GLDAS/NOAH and TRMM is clearly consistent with that of GRACE. The PCs are compared at interannual and seasonal scales as well. Note that precipitation is an instantaneous amount while water storage is a state value, so the former should be integrated in time to make it comparable to the latter. Here, we integrate precipitation in successive four months by an empirical weight function of (0.4, 0.6, 0.8, 1) and the value is attributed to the fourth month. The precipitation is assumed as the dominant driver of water storage change without considering the influence of runoff and evaporation (Humphrey et al., 2016). This is acceptable if only their temporal consistency is studied. However, long-term trends in runoff, evaporation and groundwater cannot be ignored anymore and they are differently reflected in these three products, so their trends have been removed before the comparison. The good resemblance in both the EOF_1 (spatial pattern) and PC_1 (temporal evolution) between GRACE, GLDAS/NOAH and TRMM indicates that they reflect similar geophysical processes, i.e., hydrological variations.

4.4 Method feasibility and reliability

The phase difference of 3 months is a prerequisite for this method and can be verified retrospectively. We tested different phase differences between hydrological and GS signals and decomposed them by the EOF method (refer to the supporting material). Two conclusions are obtained: only when the GS mass change peaks in May (3 months before the peak month of the hydrological signal) can our simulated result agree with the GRACE observation; the EOF decomposition can well restore both seasonal variation and the trend of the GS signal if the orthogonality is satisfied.

Only hydrological and GS signals can explain the first two modes considering their spatial and temporal patterns. Atmosphere contribution has already been removed in GRACE observations and mass transports of solid earth are unlikely to have such strong seasonal variations. We cannot quantify the contribution of groundwater, but groundwater is apt to be modulated by stronger rainfall in summer (Andermann et al., 2012), rather than snowfall in winter-spring, and groundwater activity will be reduced here in winter-spring when the ground is frozen. The negative trend in the first mode is likely due to decreasing precipitation in recent years (Figure S8) and intense groundwater pumping (Shamsudduha et al., 2012). The negative trend in the second mode is supposed to represent GS melting and can be used for estimating GS mass balance.

5. Results and discussion

5.1 Glacier and snow mass balance

225   The glacier surface elevation changes measured by the ICESat are compared with our GRACE-based estimates. We interpolate the series of GRACE estimates (2002–2016) into the observation epochs of ICESat (2003–2009) and plot mass changes (by GRACE) as a function of elevation changes (by ICESat) (Figure 6a). After divided by the glacier density, the slope of the elevation-mass regression line represents the inventorial glacierized area by RGI 6.0. The observations in October/November (blue squares) coincide with the line, indicating the good consistency between ICESat and GRACE in the

230   late ablation season between 2003 and 2009. The MODIS result indicates that the snow coverage increases rapidly since September (Figure 6b). We speculate that the snow height does not increase much in the first few months so the contribution of snow mass is not significant. The observations in March and June, as expected, are well above the line, implying an extra snow mass contribution, which can be inferred from the point-to-line vertical distance. The snow contribution relative to the total mass anomalies varies drastically between 0% and 62% with a mean value of 38% within our observation time windows.

235   The difference between GRACE and ICESat-based estimates of mass change indicates that the snowpack outside the glaciers is a non-negligible contributor to the seasonal mass variation. This is quite different from previous glacier trend estimates, where only glacierized area needs to be considered. Based on MODIS observations, the snow coverage area in this region varies from approximately 80,000 km^2 in winter to 30,000 km^2 in summer, both of which are much larger than the inventoried glacier area (Figure 6b). However, heterogeneous snow depths (Das and Sarwade, 2008) and densities across the

240   vast and rugged area make it difficult to measure their mass change by a non-gravimetric way.

Figure 6c compares the time series of glacial mass in the SETP from GRACE (Aug. 2002 to Dec. 2016) and ICESat (2003–2009). The times series from two sensors are consistent in seasonal and interannual variations, despite that the snow component is absent in the ICESat result. Monthly mass change shows that the ablation season is generally from June to October, but its initiation and duration may vary with different years (Figure 6d). The maximum mass increase (10–20 Gt)

245   usually occurs in April, when the spring precipitation peaks, and the severest mass loss (-15 – -30 Gt) usually occurs in July when the temperature peaks. With the increase of temperature from April to July, the monthly mass change curve drops steeply from the peak down to the trough, but the ascending process with mass accumulation is relatively more moderate and continuous.

We calculate annual mass increase and decrease by accumulating monthly mass change from November to May and from

250   June to October, respectively. From 2002 to 2016, the annual mass decrease ranged from -43.4 Gt to -73.1 Gt with an average of -57.6 Gt, and the annual mass increase ranged from 35.7 Gt to 63.4 Gt with an average of 50.5 Gt. The seasonal glacier and snow changes postpone the runoff of the winter-spring solid precipitation of ~50 Gt for several months. This amount plays a vital role in the annual streamflow (130.7 Gt on average) of the upper Brahmaputra (Lutz et al., 2014). Without this buffering effect, it would impose an impact ten times as large as the annual net meltwater (-6.5 Gt) does on the streamflow in summer

255   and autumn, when the water demand is high, and adaptive management on the dams in the Brahmaputra will be required to
reduce seasonal irregularities in the streamflow (Barnett et al., 2005).

5.2 Quantifying the sensitivity of glacier and snow melt to temperature

Temperature is a dominant factor influencing the melting of glaciers (Cogley et al., 2011). Here, the monthly temperature
records averaged from four meteorological stations (the red triangles in Figure 1) are compared with month-to-month mass
260   changes by GRACE to investigate the sensitivity of the GS mass balance to temperature (Figure 7). Mass changes are
negatively correlated with the temperature anomalies by a factor of -2.9 ± 0.3 Gt degree^{-1} during the ablation season (from
May to October) but no correlation is found during the accumulation season (from November to April). The mass peaks around
May, when either glacier accumulation or ablation could happen. The temperature averaged in this transitional month is taken
as the reference for the temperature anomalies used in the figure and their mass changes are annotated. We did not get a good
265   linear regression in the May results, but the glaciers in May generally experience ablation/accumulation during
positive/negative temperature anomalies and there are only 3 exceptions out of 14 cases. This implies that the initiation of the
ablation process may be temperature sensitive and that the glacier ablation period is expected to shift to an earlier time in the
case of warmer climates. The highest sensitivity of monthly mass changes in response to temperature is observed in July (4.6
Gt degree^{-1}, P-value: 0.028), when the largest monthly mass loss occurs.

270   To investigate the impact of climatic variables on the interannual variations of GS mass, we compare annual mass losses
(from May to October) with summer temperatures (from June to August) (Figure 7b). The annual mass loss is significantly
correlated with the summer temperature, with a slope of -10.3 ± 4.1 Gt degree^{-1} (P-value: 0.021, R^2-value: 0.35), indicating
that the annual GS mass balance is sensitive to summer temperature. The small value of R^2 is partly due to the relatively large
uncertainties of our mass estimate (10 Gt) in this modest range of variation (30 Gt) and the neglect of other factors influencing
275   GS mass balance. The sensitivity index was provided by a previous study (Sakai and Fujita, 2017), where the whole HMA was
examined and the SETP shows a widespread high sensitivity with an average value of -1.23 m w.e. degree^{-1}. Based on the
glacierized area of 9,679 km^2, our estimation is -1.08 ± 0.42 m w.e. degree^{-1}, which is comparable with the earlier study of
Sakai and Fujita (2017). It should be pointed out that annual net mass balance was used in Sakai and Fujita (2017) in
comparison with the annual mass loss used in this study, although annual net mass balance is mainly driven by summer melt
280   (Ohmura, 2011).

5.3 Comparison with previous estimations on glacier and snow meltwater

The trend of glacier elevation change by ICESat in this study is -0.65 ± 0.20 m w.e. yr^{-1} during 2003–2009, which lies
between the values of -0.30 ± 0.07 m w.e. yr^{-1} (Gardner et al., 2013) and -1.34 ± 0.29 m w.e. yr^{-1} (Kääb et al., 2015) in eastern
NTM by using alike ICESat dataset, and is close to the trend of -0.62 ± 0.23 m w.e. yr^{-1} during 2000–2016 by using ASTER
285   (Brun et al., 2017). The trend of GS mass change by using GRACE is -6.5 ± 0.8 Gt yr^{-1} between August 2002 and June 2017.
The mass contribution from snow is only considerable at the seasonal scale and is negligible over 15 years, so the secular trend

by using GRACE mainly represents glacier mass change. Our GRACE trend is in good consistency with the derived glacier mass change of -5.5 ± 2.2 Gt yr^{-1} by using ASTER (the area-averaged rate in NTM and Bhutan multiplied by the glacierized area of 9,679 km^2). In conclusion, both of our ICESat and GRACE estimates agree well with the previous ASTER result in

290   terms of secular trend.

      A recent result on changes in interannual glacier flow in this region (Dehecq et al., 2018) indicates a strong correlation between ice flow rate and changes in glacial thickness. The 1-year smoothed sequence of GRACE-derived mass changes in Figure 6c has no seasonal variation and reflects interannual variations. A notable feature is the balance during periods of 2003-2005 and 2011-2014. According to the previous study (Dehecq et al., 2018), thinning glaciers reduce their flow rate due to the

295   weakening gravitational driving stress; therefore, this balanced mass state may slow down the decreasing flow rate. Coincidentally, we can identify such decelerating phase during the decline of glacier flow rate during 2004-2006 and 2012-2015 (Fig. 1 in Dehecq et al., 2018).

      In our study region, 85% of its meltwater (estimated according to the area proportion) runs into the Brahmaputra and this area accounts for 83% of total glaciers in this basin (9,912 km^2). Monthly changes of meltwater estimated by month-to-month

300   difference in GRACE results are compared with model results of Lutz et al. (2014), which showed that GS melt constitutes 33% of the total discharge in the Brahmaputra and that 50% of the annual melt occurs in the summer (Figure 8). GRACE only detects the net change in GS and cannot separate mass ablation and accumulation (see the inset in Figure 8). Because these two processes concur simultaneously in transitional seasons and offset to some extent, the annual mass decrease (total mass loss in a year; here, ranges from 36.9 km^3 to 62.1 km^3 with an average of 49.0 km^3) is smaller than the realistic GS melt.

305   Therefore, we cannot accurately estimate the amount of annual GS melt each year. Instead, the amount of GS melt can be better determined during the summer (from June to August), when the accumulation is supposed to be small. This value can be used to validate the model output. Our result shows that the summer melt ranges from 31.0 km^3 to 52.2 km^3 with an average of 42.8 km^3, which is over 80% larger than the 23 km^3 GS mass change given in Lutz's model (Figure 8). Among all model estimates, Lutz's model reported one of the largest proportions of GS melt contribution (33%), but still largely underestimated

310   the amount of summer meltwater, according to our estimate from satellite observations.

      Our annual mass decrease (average 49.0 Gt) is still much smaller than the 137 Gt annual meltwater given by Huss et al. (2017). However, this enormous value even exceeds the annual streamflow of 130.7 km^3 in the upper Brahmaputra where all GS meltwater is included (Lutz et al., 2014). The upper streamflow at the Nuxia station (ahead of the main glacier supply area) is ~ 60 km^3. Therefore, the difference in streamflow between the main glacier supply area is ~ 70 km^3, and the annual meltwater

315   is unlikely to exceed this value, considering the additional contribution of precipitation. These values generally represent decadal averages at the beginning of this century (Table 1) and they are therefore comparable.

6 Conclusion

In this study, we use GRACE gravimetry to estimate the glacier and snow mass balance in the SETP from August 2002 to June 2017. The second EOF mode of GRACE observations is attributed to changes in GS mass, which can be validated in

320 the following three steps. First, simulation experiment shows that two signals with peaks in August and May can be decomposed unbiasedly by EOF. Second, the attribution of the first decomposed mode to hydrological processes can be well explained by the physical components, showing consistent spatio-temporal patterns with the soil moisture and precipitation variations from the GLDAS and TRMM data, respectively. Thirdly, the second mode of GRACE signal with a peak in May can be explained reasonably as the GS mass variation, which temporally corresponds to the glacier/snow accumulation and

325 ablation processes and spatially coincides with the glacier distribution, and is also supported by the spring precipitation pattern observed by meteorological stations. Glacier mass change measured by ICESat is further adopted to compare with our GRACE-based GS estimates, and good agreement is reached in the ablation season when the snow contribution is negligible. The ICESat measurements also show that the annual variation in glacier mass is large, which is consistent with our finding that GS mass change in this region peaks in May.

330 The decomposed GRACE time series not only shows a secular mass-decreasing trend of -6.5 ± 0.8 Gt yr^{-1}, generally comparable with previous studies on glacier mass balance in the SETP, but also newly reveals a strong seasonal variation which postpones water supply of about 50 Gt from winter and spring to summer and autumn. The high sensitivity of glacier mass changes responding to temperature shows that warming climate will exert strong impacts on the glacier and snow mass balance from two aspects. On the one hand, under the current glacier condition, the increase in summer temperature will

335 enhance the annual meltwater by a factor of -10.3 ± 4.2 Gt °C^{-1}; On the other hand, the seasonal meltwater will shift earlier and reduce its supply in summer and autumn, which is potentially ten times the amount of annual glacier melting. Our estimates of monthly GS meltwater can also give an elaborate calibration on the glacier accumulation and ablation processes in hydrological and glaciological models of the Brahmaputra Basin, which were only calibrated indirectly by sparsely sampled streamflow discharges and diverged largely on the proportion of seasonal meltwater contribution. The vulnerability of the

340 Brahmaputra streamflow to warming temperatures is higher than previously recognized, suggesting that there will be ominous tension in the allocation of its water resource in the future.

Data availability

The data that support this study are mostly publicly open and their sources are indicated in the data section. The meteorological data and the series of glacier mass balance estimate are available upon request to the corresponding author.

345 **Author contributions**

S.Y. conceived the study and conducted the calculations. S.Y. and C.S. analyzed the results and wrote the manuscript. K.H. discussed and revised the manuscript. S.K. discussed and suggested the experiment. Q.W. processed the ICESat data. L.C. processed the MODIS data.

Competing financial interest

350   The authors declare no competing financial interests.

Acknowledgments

S.Y. is supported by JSPS KAKENHI Grant Number JP16F16328 and the Alexander von Humboldt Foundation. C.S. is supported by the Strategic Priority Research Program of the Chinese Academy of Sciences (grant no. XDA23100102) and the National Key R and D Program of China (grant no. 2018YFD1100101, 2018YFD0900804)

355

References

A, G., Wahr, J., and Zhong, S.: Computations of the viscoelastic response of a 3-D compressible Earth to surface loading: an application to Glacial Isostatic Adjustment in Antarctica and Canada. Geophys. J. Int., 192(2), 557-572, 2013.

Andermann, C., Longuevergne, L., Bonnet, S., Crave, A., Davy, P., and Gloaguen, R. : Impact of transient groundwater storage
360   on the discharge of Himalayan rivers. Nat. Geosci., 5(2), 127, 2012.

Barnett, T. P., Adam, J. C., and Lettenmaier, D. P.: Potential impacts of a warming climate on water availability in snow-dominated regions. Nature, 438, 303. doi: 10.1038/nature04141, 2005.

Björnsson, H., and Venegas, S.: A manual for EOF and SVD analyses of climatic data. CCGCR Report, 97(1), 112-134, 1997.

Bolch, T., Kulkarni, A., Kaab, A., Huggel, C., Paul, F., Cogley, J. G., . . . Stoffel, M.: The State and Fate of Himalayan Glaciers.
365   Science, 336(6079), 310-314. doi: 10.1126/science.1215828, 2012.

Bookhagen, B., and Burbank, D. W.: Toward a complete Himalayan hydrological budget: Spatiotemporal distribution of snowmelt and rainfall and their impact on river discharge. J. Geophys. Res., 115(F3). doi: 10.1029/2009jf001426, 2010.

Brun, F., Berthier, E., Wagnon, P., Kääb, A., and Treichler, D.: A spatially resolved estimate of High Mountain Asia glacier mass balances from 2000 to 2016. Nat. Geos. doi: 10.1038/ngeo2999, 2017.

370   Chen, J. L., Wilson, C. R., Li, J., and Zhang, Z.: Reducing leakage error in GRACE-observed long-term ice mass change: a case study in West Antarctica. J. Geodesy, 89(9), 925-940. doi: 10.1007/s00190-015-0824-2, 2015.

Chen, X., Long, D., Hong, Y., Zeng, C., and Yan, D.: Improved modeling of snow and glacier melting by a progressive two-stage calibration strategy with GRACE and multisource data: How snow and glacier meltwater contributes to the runoff of the Upper Brahmaputra River basin? Water Resour. Res., 53(3), 2431-2466, 2017.

375   Cheng, M., Ries, J. C., and Tapley, B. D.: Variations of the Earth's figure axis from satellite laser ranging and GRACE. J. Geophys. Res., 116(B1). doi: 10.1029/2010jb000850, 2011.

Cogley, J., Hock, R., Rasmussen, L., Arendt, A., Bauder, A., Braithwaite, R., and Nicholson, L.: Glossary of glacier mass balance and related terms. IHP-VII technical documents in hydrology, 86, 965, 2011.

Das, I., and Sarwade, R.: Snow depth estimation over north-western Indian Himalaya using AMSR-E. Int. J. Remote Sens.,
380   29(14), 4237-4248, 2008.

Dehecq, A., Gourmelen, N., Gardner, A. S., Brun, F., Goldberg, D., Nienow, P. W., and Trouvé, E.: Twenty-first century glacier slowdown driven by mass loss in High Mountain Asia. Nat. Geos., 12(1), 22-27. doi: 10.1038/s41561-018-0271-9, 2018.

Farr, T. G., Rosen, P. A., Caro, E., Crippen, R., Duren, R., Hensley, S., and Roth, L.: The shuttle radar topography mission. Rev. Geophys., 45(2), 2007.

Gardelle, J., Berthier, E., Arnaud, Y., and Kääb, A.: Region-wide glacier mass balances over the Pamir-Karakoram-Himalaya during 1999andndash;2011. The Cryosphere, 7(4), 1263-1286. doi: 10.5194/tc-7-1263-2013, 2013.

Gardner, A. S., Moholdt, G., Cogley, J. G., Wouters, B., Arendt, A. A., Wahr, J., and Paul, F.: A Reconciled Estimate of Glacier Contributions to Sea Level Rise: 2003 to 2009. Science, 340(6134), 852-857. doi: 10.1126/science.1234532, 2013.

Hall, D., Salomonson, V., and Riggs, G.: MODIS/Terra snow cover daily L3 global 500m grid. Version 5. Boulder, Colorado USA: National Snow and Ice Data Center, 2006.

Huffman, G., Bolvin, D., Braithwaite, D., Hsu, K., Joyce, R., and Xie, P.: Tropical Rainfall Measuring Mission (TRMM) (2011), TRMM (TMPA/3B43) Rainfall Estimate L3 1 month 0.25 degree x 0.25 degree V7, Greenbelt, MD, Goddard Earth Sciences Data and Information Services Center (GES DISC). Retrieved from: http://dx.doi.org/10.5067/TRMM/TMPA/MONTH/7, 2014.

Humphrey, V., Gudmundsson, L., and Seneviratne, S. I.: Assessing Global Water Storage Variability from GRACE: Trends, Seasonal Cycle, Subseasonal Anomalies and Extremes. Surv. Geophys., 37(2), 357-395. doi: 10.1007/s10712-016-9367-1, 2016.

Huss, M.: Density assumptions for converting geodetic glacier volume change to mass change. The Cryosphere, 7(3), 877-887, 2013.

Huss, M., Bookhagen, B., Huggel, C., Jacobsen, D., Bradley, R. S., Clague, J. J., . . . Winder, M.: Toward mountains without permanent snow and ice. Earth's Future, 5(5), 418-435. doi: doi:10.1002/2016EF000514, 2017.

Immerzeel, W. W., Van Beek, L. P., and Bierkens, M. F.: Climate change will affect the Asian water towers. Science, 328(5984), 1382-1385, 2010.

Jansson, P., Hock, R., and Schneider, T.: The concept of glacier storage: a review. J. Hydrol., 282(1), 116-129. doi: https://doi.org/10.1016/S0022-1694(03)00258-0, 2003.

Kääb, A., Berthier, E., Nuth, C., Gardelle, J., and Arnaud, Y.: Contrasting patterns of early twenty-first-century glacier mass change in the Himalayas. Nature, 488(7412), 495-498. doi: 10.1038/nature11324, 2012.

Kääb, A., Treichler, D., Nuth, C., and Berthier, E.: Brief Communication: Contending estimates of 2003–2008 glacier mass balance over the Pamir–Karakoram–Himalaya. The Cryosphere, 9(2), 557-564. doi: 10.5194/tc-9-557-2015, 2015.

Kaser, G., Großhauser, M., and Marzeion, B.: Contribution potential of glaciers to water availability in different climate regimes. P. Natl. Acad. Sci. USA, 2010.

Kusche, J., Schmidt, R., Petrovic, S., and Rietbroek, R.: Decorrelated GRACE time-variable gravity solutions by GFZ, and their validation using a hydrological model. J. Geodesy, 83(10), 903-913. doi: 10.1007/s00190-009-0308-3, 2009.

415   Li, X., Wang, L., Chen, D., Yang, K., Xue, B., and Sun, L.: Near-surface air temperature lapse rates in the mainland China during 1962-2011. J. Geophys. Res.: Atmospheres, 118(14), 7505-7515. doi: 10.1002/jgrd.50553, 2013.

Lutz, A. F., Immerzeel, W. W., Shrestha, A. B., and Bierkens, M. F. P.: Consistent increase in High Asia's runoff due to increasing glacier melt and precipitation. Nat. Clim. Change, 4(7), 587-592. doi: 10.1038/Nclimate2237, 2014.

Matsuo, K., and Heki, K.: Time-variable ice loss in Asian high mountains from satellite gravimetry. Earth Planet. Sc. Lett., 420   290(1-2), 30-36. doi: 10.1016/j.epsl.2009.11.053, 2010.

Maussion, F., Scherer, D., Mölg, T., Collier, E., Curio, J., and Finkelnburg, R.: Precipitation seasonality and variability over the Tibetan Plateau as resolved by the High Asia Reanalysis. J. Climate, 27(5), 1910-1927, 2014.

Ohmura, A.: Observed Mass Balance of Mountain Glaciers and Greenland Ice Sheet in the 20th Century and the Present Trends. Surv. Geophys., 32(4), 537-554. doi: 10.1007/s10712-011-9124-4, 2011.

425   RGI Consortium.: Randolph Glacier Inventory – A Dataset of Global Glacier Outlines: Version 6.0: Technical Report, Global Land Ice Measurements from Space, Colorado, USA. Digital Media, 2017.

Rodell, M., Houser, P. R., Jambor, U., Gottschalck, J., Mitchell, K., Meng, C. J., . . . Toll, D.: The Global Land Data Assimilation System. B. Am. Meteorol. Soc., 85(3), 381-394. doi: 10.1175/bams-85-3-381, 2004.

Sakai, A., and Fujita, K.: Contrasting glacier responses to recent climate change in high-mountain Asia. Sci. Rep., 7(1), 13717. 430   doi: 10.1038/s41598-017-14256-5, 2017.

Shamsudduha, M., Taylor, R., and Longuevergne, L.: Monitoring groundwater storage changes in the highly seasonal humid tropics: Validation of GRACE measurements in the Bengal Basin. Water Resour. Res., 48(2), 2012.

Swenson, S., Chambers, D., and Wahr, J.: Estimating geocenter variations from a combination of GRACE and ocean model output. J. Geophys. Res.: Solid Earth (1978–2012), 113(B8), 2008.

435   Swenson, S., and Wahr, J.: Post-processing removal of correlated errors in GRACE data. Geophys. Res. Lett., 33(8). doi: 10.1029/2005gl025285, 2006.

Tanck, R., and Fazani, A.: Damming Tibet's Yarlung Tsangpo-Brahmaputra and other South Asian rivers. Retrieved May 5, 2019, from http://tibetanplateau.blogspot.com/2010/05/damming-tibets-yarlung-tsangpo.html, 2010.

Tapley, B. D., Bettadpur, S., Ries, J. C., Thompson, P. F., and Watkins, M. M.: GRACE measurements of mass variability in 440   the Earth system. Science, 305(5683), 503-505, 2004.

Treichler, D., and Kääb, A.: Snow depth from ICESat laser altimetry—A test study in southern Norway. Remote Sens. Environ., 191, 389-401, 2017.

Wang, Q., Yi, S., Chang, L., and Sun, W.: Large-Scale Seasonal Changes in Glacier Thickness Across High Mountain Asia. Geophys. Res. Lett., 44, 10427-10435, 2017.

445   Wouters, B., Chambers, D., and Schrama, E. J. O.: GRACE observes small-scale mass loss in Greenland. Geophys. Res. Lett., 35(20). doi: 10.1029/2008gl034816, 2008.

Wu, G., Guan, Y., Liu, Y., Yan, J., and Mao, J.: Air–sea interaction and formation of the Asian summer monsoon onset vortex over the Bay of Bengal. Clim. Dynam., 38(1-2), 261-279. doi: 10.1007/s00382-010-0978-9, 2011.

Yang, W., Yao, T., Guo, X., Zhu, M., Li, S., and Kattel, D. B.: Mass balance of a maritime glacier on the southeast Tibetan
450   Plateau and its climatic sensitivity. J. Geophys. Res.: Atmospheres, 118(17), 9579-9594. doi: 10.1002/jgrd.50760, 2013.

Yao, T., Thompson, L., Yang, W., Yu, W., Gao, Y., Guo, X., and Joswiak, D.: Different glacier status with atmospheric
circulations in Tibetan Plateau and surroundings. Nat. Clim. Change, 2(9), 663-667. doi: 10.1038/nclimate1580, 2012.

Yi, S., and Sun, W.: Evaluation of glacier changes in high-mountain Asia based on 10 year GRACE RL05 models. J. Geophys.
Res.: Solid Earth, 119(3), 2504-2517. doi: 10.1002/2013jb010860, 2014.

455   Yi, S., Sun, W., Feng, W., and Chen, J.: Anthropogenic and climate-driven water depletion in Asia. Geophys. Res. Lett.,
43(17), 9061-9069, 2016.

Zhang, L. L., Su, F. G., Yang, D. Q., Hao, Z. C., and Tong, K.: Discharge regime and simulation for the upstream of major
rivers over Tibetan Plateau. J. Geophys. Res.-Atmospheres, 118(15), 8500-8518. doi: 10.1002/jgrd.50665, 2013.

460
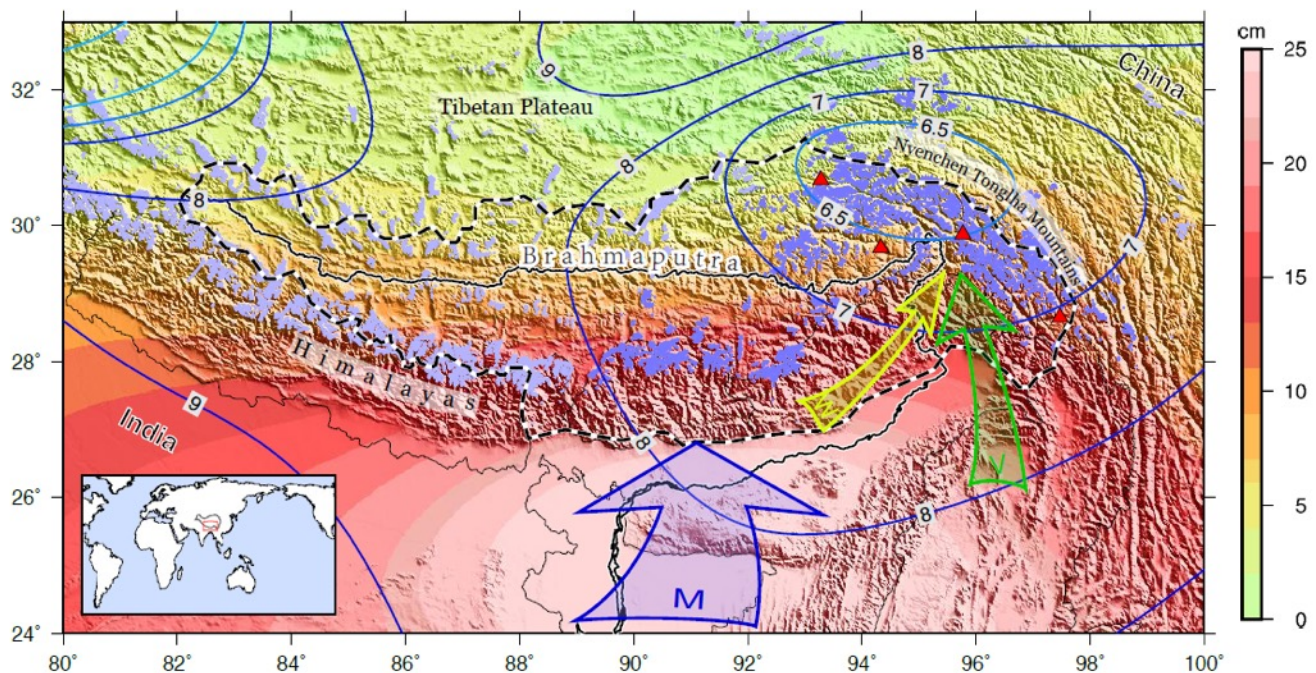
Figure 1. Geographic environment of the upper Brahmaputra Basin. The boundary of the basin is outlined by the black dashed line. The violet areas in the plateau represent mountain glaciers, but only the darker ones (9,679 km² in total) are studied here. The background color shows the amplitudes of annual variation in terms of equivalent water height from GRACE, and their peak months (the month with the peak value in a year) are indicated using contours (e.g. 9 means September). The red triangles mark the location of four meteorological stations. The colored arrows illustrate major climatic factors influencing this region (M: Indian Monsoon; W: Westerly winds; V: Bay of Bengal Vortex). The red box in the inset map marks the location of the study area.

465
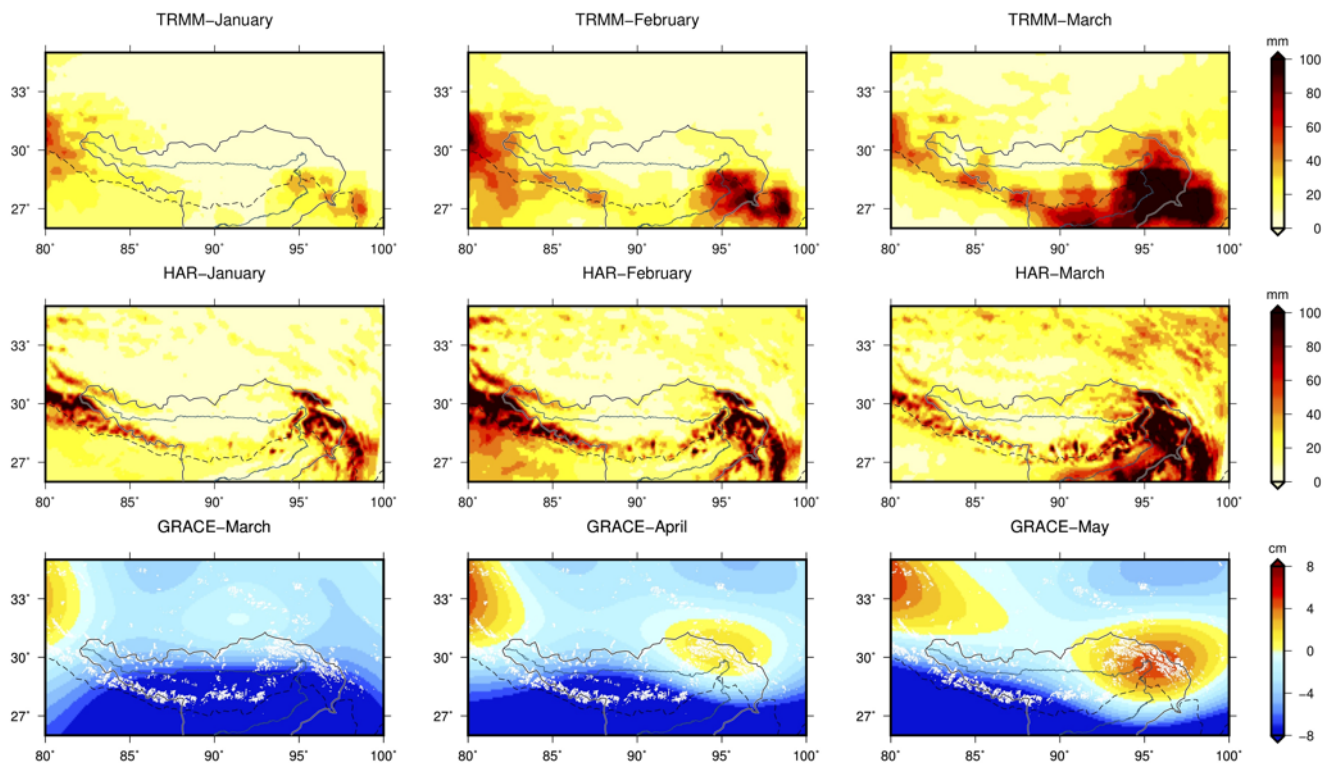
Figure 2. Monthly precipitation from January to March by TRMM and HAR and mass anomalies from March to May by GRACE. The Brahmaputra and its basin boundary are marked. The white dots in the bottom plots represent glaciers.

a

b
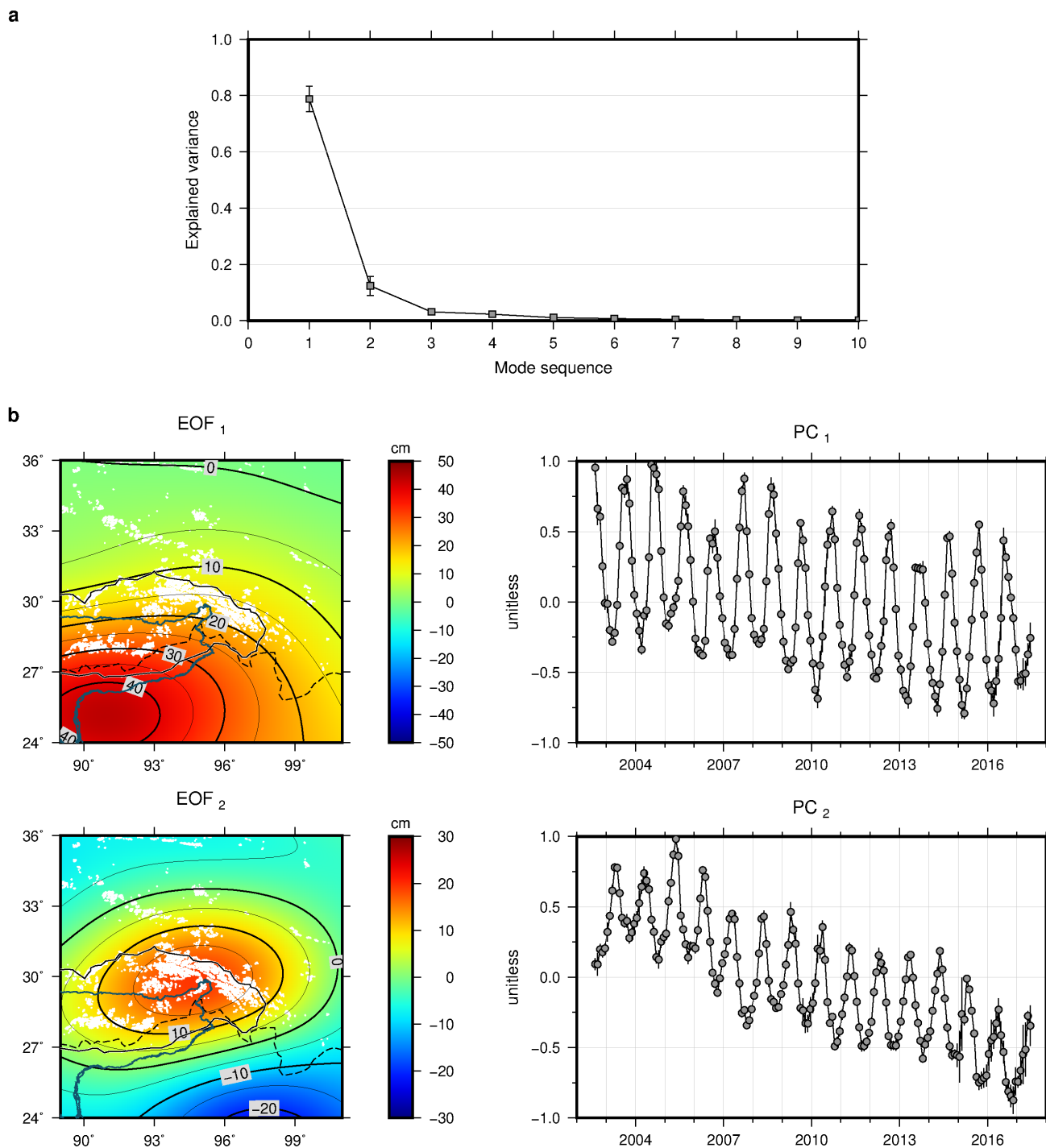
Figure 3. EOF decomposition of GRACE observations in the form of EWH in the study region. Six combinations are averaged to generate these plots and uncertainties are estimated based on the dispersions. (a) Weight of the first 10 components. (b) Spatial distribution (EOF) and temporal variation (PC) of the first two components. The white dots represent locations of glaciers.

475
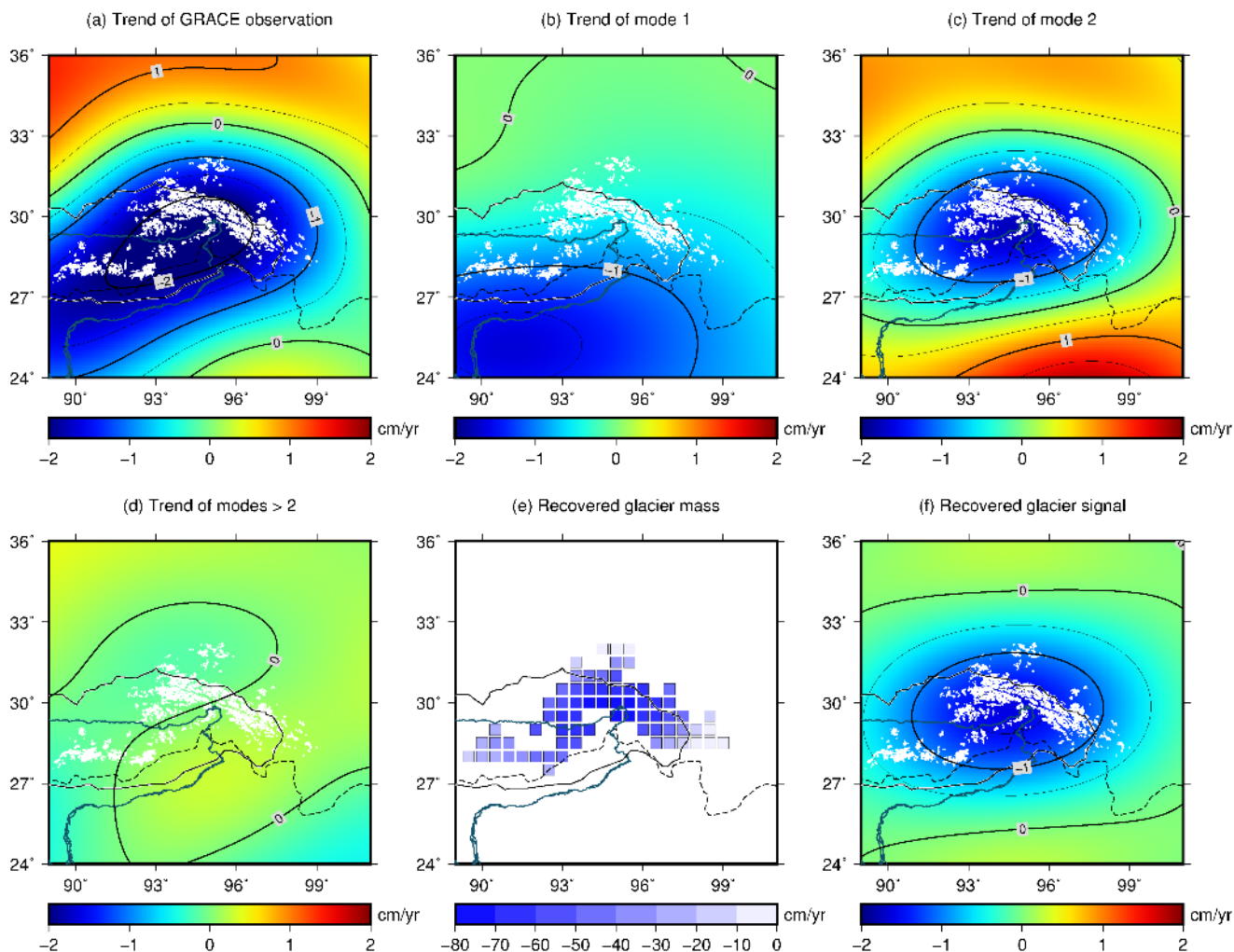
Figure 4. Trend of GRACE signals and the GS mass estimation. The CSR product with DDK4 filter is used here. (a) the trend of GRACE EWH observations between Aug 2002 and June 2017, is decomposed into (b), (c) and (d). Using the mass changes shown in (e), we obtained (f) by the forward modelling method to reproduce (c). The white dots represent glacier distribution. The black solid curve marks the basin boundary and the dashed curve marks the plateau boundary.
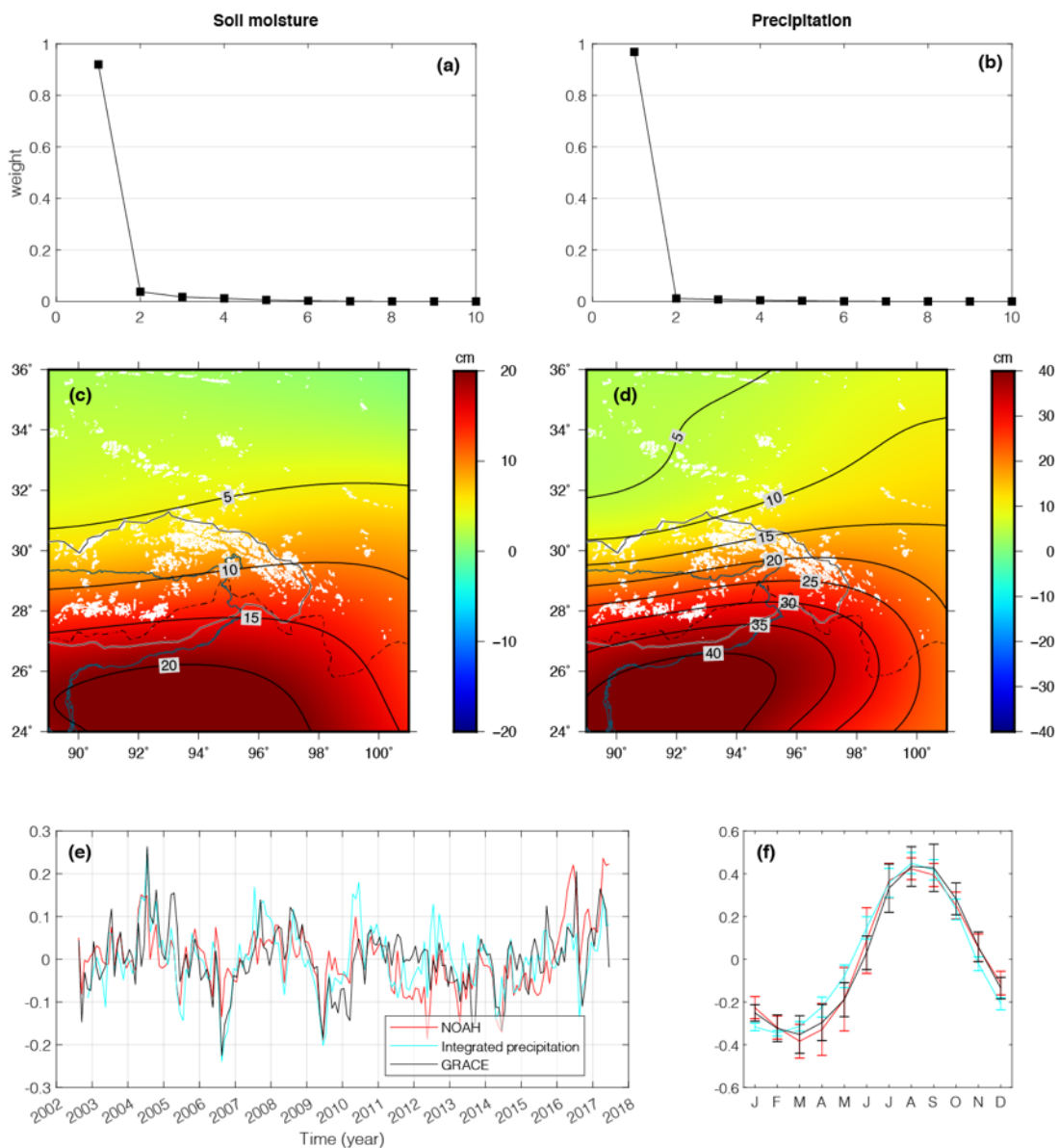
485   **Figure 5. EOF analysis of soil moisture using GLDAS/NOAH (a, c) and of precipitation using TRMM (column, d). The weights of the first 10 modes are shown in the upper panels. The first EOFs and PCs are shown in the middle and bottom panels. The PCs are separated into detrended interannual (e) and annual (f) for better comparison.**
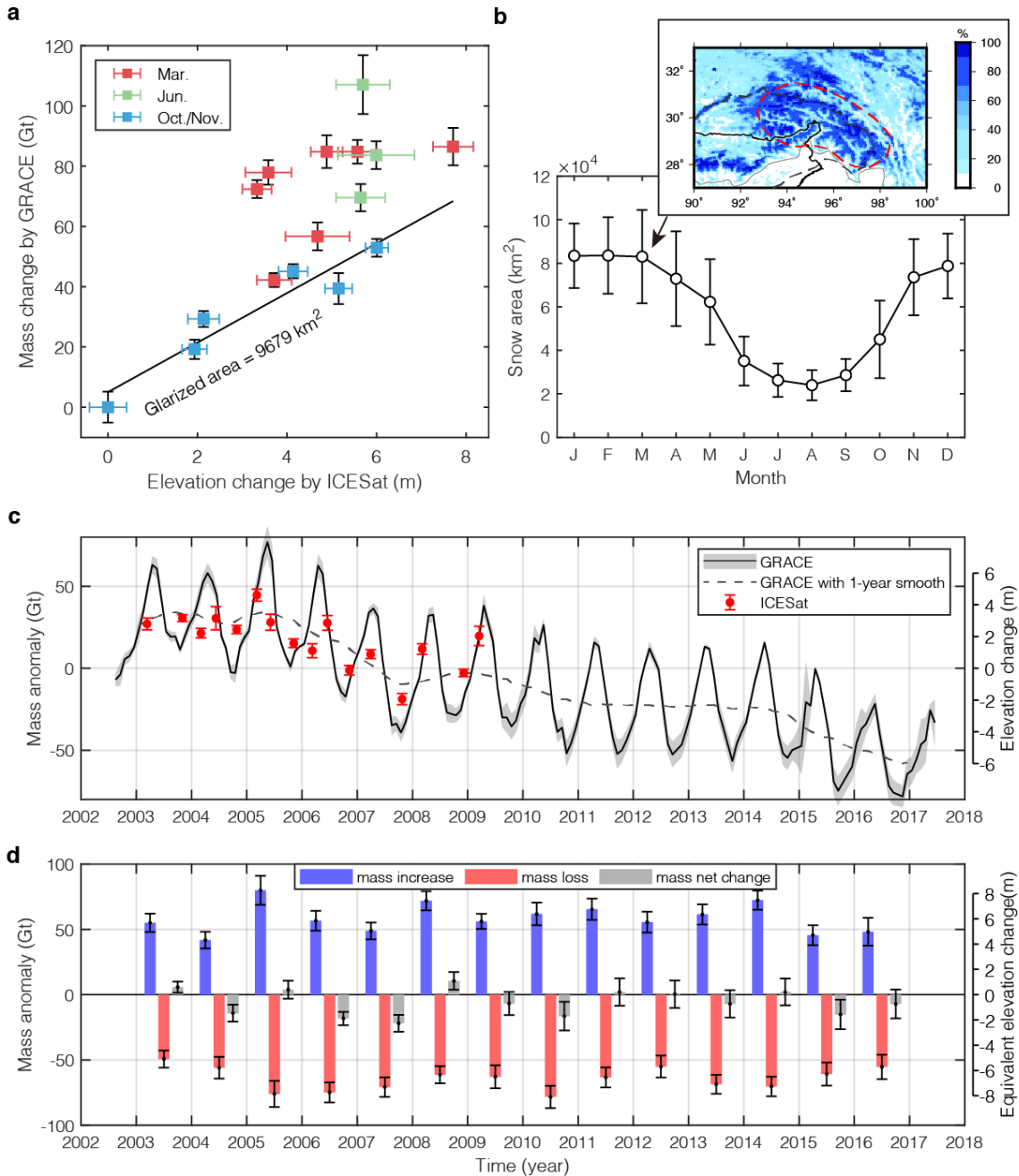
490 **Figure 6. GS mass balance in the SETP. (a) GS mass change by GRACE as a function of elevation change from ICESat. The values are anomalies relative to the minimum in October 2007. (b) Seasonal snow coverage changes. The error bars are calculated by the dispersions in the same month among years from 2003 to 2016. The coverage in March is given in the inset. The red dashed circle marks the region used for the calculation of snow area. (c) Time series of GS mass change estimated by GRACE and glacier mass change by ICESat. The glacierized area of 9,679 km² is used to convert thickness change into mass change. (d) Annual mass**
495 **increase/decrease from 2003 to 2016 by GRACE.**
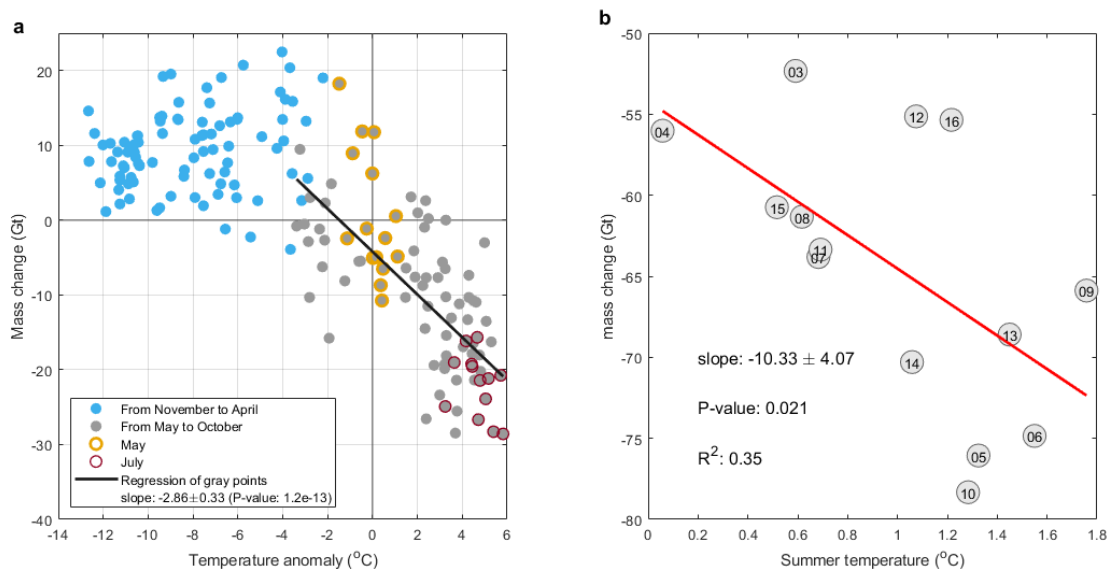
Figure 7. Regression between mass change and temperature. (a) Monthly mass changes as a function of monthly temperature anomalies. (b) Linear regression between annual mass decreases and summer temperatures. The number in the circle represents the year of the data (e.g. "15" shows 2015).
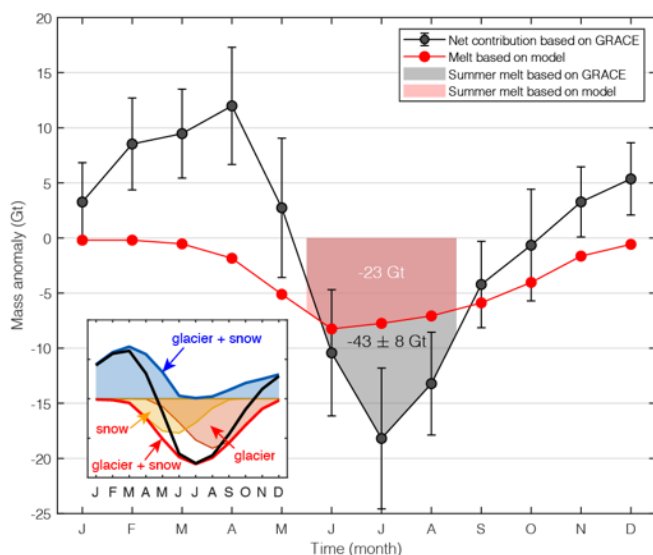
Figure 8. Monthly mass change from GS in the upper Brahmaputra Basin estimated by GRACE and by the model of Lutz et al. (2014). Negative values mean a net increase of meltwater (i.e., more glacier and snow melt than accumulation). Note that Lutz's model only estimated the melt component, while GRACE detects the net change including both melt and accumulation. The estimates

of summer melt are annotated. A schematic diagram of seasonal mass balance is shown in the inset (Blue text represents mass accumulation, red represents ablation, and the black curve represents the net change).

Table 1. Previous model-based estimates of meltwater contribution to the Brahmaputra discharge.

Study literature	Time span	Drainage area (km²)	Amount of meltwater (w.e. km³ yr⁻¹)	Total discharge (km³ yr⁻¹)	Meltwater/total discharge (%)
Immerzeel et al. 2010	2000–2007	525,797	62	230	27
Bookhagen and Burbank, 2010	1998–2007	255,929	55	161	34
Zhang et al., 2013	1961–1999	201,200*	20	58	35
Lutz et al., 2014	1998–2007	360,000	43	131	34
Huss et al., 2017	2002–2011**	533,000	138	732	19
Chen et al., 2017b	2003–2014	240,000*	12	60	21

510   * The NTM is almost not included.

    ** The time spans vary a bit in different datasets.